Development of an adaptive multi-method algorithm for automatic picking of first arrival times: application to near surface seismic data

Amin Khalaf, Christian Camerlynck, Nicolas Florsch, Ana Schneider

Development of an adaptive multi-method algorithm for automatic picking of first arrival times: application to near surface seismic data

Amin Khalaf (1, 2), Christian Camerlynck (1), Nicolas Florsch (3) and Ana Schneider (1).

(1) Sorbonne Université, EPHE, Milieux Environnementaux, Transferts et Interactions dans les hydrosystèmes et les Sols, METIS, F-75005 Paris, France.

(2) Tishreen University, Faculty of Sciences, Departement of Geology, Lattakia, Syria.

(3) Sorbonne Université, IDR, UMI 209 Ummisc, F-75005 Paris, France.

Corresponding author:

Amin Khalaf

UPMC, METIS.

Case 105, 4 place Jussieu, 75005 Paris, France.

Phone : +33 (0)1 44 27 48 85

Fax : +33 (0)1 44 27 45 88

E-mail address: amin.khalaf@upmc.fr

ABSTRACT

Accurate picking of first arrival times plays an important role in many seismic studies, particularly in seismic tomography and reservoirs or aquifers monitoring. Many techniques have been developed, mainly for seismological purposes, in order to pick first arrivals automatically or semi-automatically. However, these techniques do not reach the accuracy required in shallow seismic due to the complexity of near surface structures and low signal-to-noise ratio. We propose here a new adaptive algorithm to automatically pick first arrival in near surface seismic data by combining three picking methods: Multi-Nested Windows, Higher Order Statistics, and Akaike Information Criterion. They benefit from combining different properties of the signal in order to highlight first arrivals and finally provide an efficient and robust automatic picking. This strategy mimics the human first-break picking, where a global trend is first defined at the beginning of the picking procedure. The exact first-breaks are then sought in the vicinity of each point suggested by this trend. Three successive phases are combined in a multistage algorithm, each of them characterizing a specific signal property. Within each phase, the potential picks and their error range are automatically assessed and sequentially used as prior in the following phase picking. Since having realistic estimates of the error in picked traveltimes is crucial for seismic tomography, our adaptive algorithm automatically provides picked arrivaltimes with their associated uncertainties. We demonstrate the accuracy and robustness of the implemented algorithm with synthetic, pseudo-synthetic, and real datasets presenting challenges for classical automatic pickers. The comparison of both manual and adaptive picking procedures demonstrates that our new scheme provides more reliable results even under different noisy conditions. All parameters of our multi-method algorithm are self-adaptive thanks to the sequential integration of each sub-algorithm results in the workflow.

Hence, it is nearly a parameter-free algorithm, which is straightforward to implement and demands low computational resources.

Keywords: automatic picking, adaptive algorithm, multi-nested window, kurtosis, Akaike Information Criterion, seismic tomography, look-like Monte Carlo.

INTRODUCTION

Seismic arrival-time picking is crucial for many seismological studies. Using picked arrival-times, we can locate earthquakes, understand the interior structure of the Earth, study the geotectonic context and evaluate seismic risk for a region (Billings et al., 1994; Hafez et al., 2009; Ross and Ben-Zion, 2014; Stewart, 1977). More specifically in reflection and refraction seismology, first-arrival times are picked to guess the near-surface structure (Blias, 2012; Lanz et al., 1998; Lawton, 1989). The quality of inverted models (near-surface layers' velocity and thickness) therefore depends on the accuracy of the picked first-arrival times (Senkaya and Karslı, 2014) since a small error in times may result in a non-negligible error in velocity and depth calculations (Ramananantoandro and Bernitsas, 1987).

The first events can be classically defined as the first remarkable onset of seismic energy, i.e. “the first noticeable departure of the seismic pulse from a background signal” (Hatherly, 1982). However, they do manifest themselves as a noticeable variation in amplitude, frequency content, statistical properties, and/or polarization properties in time and/or frequency domain. The quality of these events depends on the source type and near-surface conditions (Yilmaz, 2001). The ambient noise may over-shadow the early part of the seismic phase and delay its apparent occurrence.

Traditionally, the first arrival times are manually picked by human operators, but the huge volume of data (especially in active-source seismic applications) makes this visual handpicking tedious, time-consuming and thus inefficient. Furthermore, the subjectivity of human-eye picking (Hatherly, 1982; Jiao and Moon, 2000) puts alongside with factors relative to the operator's physiological and/or psychological state make the results of manual picking results often biased or inconsistent (Saragiotis et al., 2002; Sabbione and Velis, 2010).

On the other hand, automatic picking is a more objective tool since it allows rapid analysis of large data sets while providing homogeneous and consistent results. Computer-based picking methods can be divided into semi-automatic (e.g. Lou et al., 2013; VanDecar and Crosson, 1990) and full-automatic (e.g. Coppens, 1985; Küperkoch et al., 2010; Lomax et al., 2012) algorithms. These algorithms can be further classified into two main approaches: single-trace and multi-trace. Single-trace algorithms can be either used as a "detector" in order to recognize a seismic phase arrival, or as a "picker" in order to determine a precise onset time of a detected phase (Allen, 1982). Multi-trace algorithms can be seen as an extension of single-trace algorithm, working on several traces at once. They are usually used for picking passive and active-source seismic data, benefiting from the similarity of waveforms from nearby events. Recently, Tselentis et al. (2012) provided an excellent classification of the common event-detection and phase-picking methodologies. Another exhaustive review with a new classification (i.e. single-level, hybrid and multi-level algorithms) was recently provided by Akram and Eaton (2016a) with discussion about the key parameters of each algorithm on downhole microseismic data. Among these algorithms, the most reported for single-trace (P-, S-phase, or both) picking are energy ratio criteria (STA/LTA) (Allen, 1982, 1978; Baer and Kradolfer, 1987; Earle and Shearer, 1994), autoregressive-Akaike information criteria (AIC) (Maeda, 1985; Sleeman and van Eck, 1999; Takanami and Kitagawa, 1988), higher order statistics (HOS) (Saragiotis

et al., 2004, 2002), polarization information (Cichowicz, 1993), and wavelet transform (WT) (Anant and Dowla, 1997; Bogiatzis and Ishii, 2015; Zhang et al., 2003).

Although a multitude of algorithms exists, the aforementioned automatic methods are less commonly used in the literature for first-arrival picking on near-surface refraction records. Peraldi and Clement (1972) proposed an algorithm based on cross correlation of the seismic trace with a reference "model" trace. However due to incorrect assumption about waveform stationarity, this algorithm does not pick the first arrivals accurately (Gelchinsky and Shtivelman, 1983). Hatherly (1982) proposed an algorithm combining the correlation method with a linear least-squares prediction method. A drawback of this algorithm is that it is non-robust against random noise. Gelchinsky and Shtivelman (1983) used a method based on spatial correlation properties of the refracted signals. To prevent an apparent cycle skipping problem with the cross correlation approach, Zelt et al. (1987) implemented a Monte Carlo technique in which the cross correlation function is transformed into a probability distribution using semblance optimization in order to pick low amplitude arrivals in crustal refraction data. Like other automatic picking methods, the accuracy of cross-correlation based methods decreases with the signal-to-noise ratio (SNR). However, the accuracy of these algorithms may be improved when combined with (i) semi-automatic processes in which human operators can interactively guide the algorithm to the correct pick (e.g. Senkaya and Karslı, 2014), (ii) iterative stacking/filtering procedures that leads to improve SNR signals (e.g. Akram and Eaton, 2016b; Iqbal et al., 2017), (iii) or both (e.g. Lou et al., 2013; Pavlis and Vernon, 2010).

Data pre-processing can also improve the detectability of first arrivals and increase the accuracy of automatic picking (Mousa et al., 2011; Mousa and Al-Shuhail, 2012). In strong heterogeneous velocity fields, the first arrivals do not necessarily correspond to the most energetic wavefield

(Geoltrain and Brac, 1993), especially in the case of refracted arrivals at far offsets. Therefore, seismic noise can considerably impede automatic picking of weak (Tselentis et al., 2012). One way to address this problem is to filter the data before automatic picking. But when the first arrivals and noise share the same frequency band, data filtering becomes ineffective for automatic picking. Allam et al. (2014) showed the potential effects of causal and non-causal filters on head wave picking quality. Non-causal filters can introduce small artifacts ringing to the front of high-amplitude arrivals, whereas causal filters can produce a phase shift. Additionally, Aldersons (2004) and Senkaya and Karslı (2014) discussed the troublesome effects inherent to the choice of corner frequencies and slopes of a filter .

The combination of multi-methods was also proposed to increase the accuracy of automatic techniques when picking more complicated phases (e.g. S-phase) (Ross and Ben-Zion, 2014; Diehl et al., 2009; Küperkoch et al., 2012). Since each method is based on identifying a specific property of the part of the seismic trace where the first arrival occurs, the hybrid algorithms combine the advantageous properties of each individual method.

In near-surface seismic tomography, picking far offset traces remains a challenge. When picked, the overall bad quality of far offsets traveltimes usually degrades the inversion reliability though they are required to increase the investigation depth. To mitigate such effects, first arrivaltimes can be used with their associated uncertainty estimate in order to balance the trade-off between investigation depth and inversion quality. According to Aldersons (2004), estimating picking uncertainties is the second most important goal in an automatic picking algorithm. Di Stefano et al. (2006) automatically estimated the uncertainties of first arrivals by using quality weighting algorithm which takes into account the waveform sampling rate, spectral density analysis and SNR. Diehl et al.

(2009) obtained a robust estimate of error intervals for automatically picked S-arrivals by combining picking information from different methods (STA/LTA detector, polarization detector, and autoregressive picker). Küperkoch et al. (2010) introduced an automatic quality estimation of picked P-onset from local slope and SNR of the characteristic function (CF) used in their picking procedure.

Although using combined algorithms has become a standard approach for automatic picking in deep seismology, it is still not common for near surface seismic data.

Here we propose a new adaptive algorithm based on the combination of three picking methods, respectively Multi-Nested Windows (MNW), Higher Order Statistics (HOS), and Akaike Information Criterion (AIC). This work focuses on overcoming most of the shortcomings inherent to the use of a single picking method. It also aims at providing accurate P-wave arrivaltimes along with their uncertainties, which are required information for reliable near surface tomography processing. Exploiting all sub-algorithms in a single scheme proves to be beneficial in order to avoid filtering. The proposed new scheme is thus auto-adaptive and nearly parameter-free algorithm. Furthermore, all sub-algorithms are applied on raw single-component records in time domain in order to improve computational efficiency.

METHODOLOGY

Principle and methods

Most of automatic picking techniques rely on different noise and signal properties in time or/and frequency domain. The transition point (noise to signal) can be identified with an algorithm that enhances and detects a specific attribute. Our proposed strategy is based upon an adaptive algorithm combining three picking methods (MNW, HOS, and AIC). The implemented algorithm

mimics the human first-break picking, where at the beginning a global trend is defined, and then the precise first arrival times are searched in the vicinity of this trend. The picking is performed using a three stage algorithm that combines sequentially the three sub-algorithms. In this section, we describe the mathematical background of the three methods and their implementation in adaptive workflow either for a trace-by-trace or a shot-gather picking. To better illustrate and facilitate the comparison, each trace is normalized to its maximum amplitude before any process.

Multi-Nested Windows (MNW) method

The particles motion increases gradually when the disturbance of the seismic waves arrives, so usually no sudden take-off in the trace at the first break can be noticed (Ricker, 1953). Therefore, the early advent of the first arrival (here, P-wave) is usual low, and the later one would be more energetic. However, in near surface prospection, first arrivals could be obscured by ambient noise. This case is commonly met at far offsets due to the spherical divergence of the front wave, the attenuation and the interference with background noise (Mallinson et al., 2011).

Let $a(t)$ represent the amplitudes of trace at a time t ($t \in [1, N]$, of N samples). The average energy in the before, after and delayed windows (respectively $BEA,\ AEA,\ and\ DEA$) are defined by **Eq.** (1):

$$BEA(t) = \frac{1}{L_b} \int_{t-L_b}^{t} a^2(\tau) d\tau$$

$$AEA(t) = \frac{1}{L_a} \int_{t}^{t+L_a} a^2(\tau) d\tau \quad (1)$$

$$DEA(t) = \frac{1}{L_d} \int_{t+d}^{t+d+L_d} a^2(\tau) d\tau,$$

where L_b, L_a and L_d are the lengths (here in samples) of the corresponding windows in terms of dominant period length (T_d) of the first arrival wave; d is the time delay for shifting the DEA window. Trnkoczy (2012) quantified the tradeoffs between the windows size and trigger sensitivity of the short-term average/long-term average (STA/LTA; Allen, 1978) algorithm. It is claimed that the preceding window should be a few times longer than the later window for microseismic data picking (Chen, 2005; Han et al., 2009; Wong et al., 2009). In this work, the lengths of the windows are $L_b = 4T_d$, $L_a = T_d$, $L_d = (1-d)T_d$, $d = 0.6T_d$. The energy ratios ER_1 and ER_2 are defined by **Eq.** (2).

$$ER_1(t) = \frac{AEA(t)}{BEA(t) + \beta}$$

$$ER_2(t) = \frac{DEA(t)}{BEA(t) + \beta}, \quad (2)$$

where β is a constant used to avoid numerical instability in the energy ratio computation. In this study, β was adopted as 0.005 being suitable for the datasets used. It is noticed that ER_1 is slightly equivalent to energy ratio (ER=STA/LTA) methods (e.g. Han et al., 2009). However, when ER exceeds a pre-defined threshold, the first arrival is considered as detected. But the onset picking

may need further processing. Wong et al. (2009) showed that the onset of the first arrival is very close to the maximum derivative of ER. In the case of noisy traces, the first-break times derived from ER technique are somewhat later (Gaci, 2014). To overcome the problems due to first arrival weakness, we propose a new characteristic function (CF_{mnw}) by summing the two energy ratios (ER_1, ER_2), calculated in the nested windows shown in **Fig**. **1**a, as follows.

$$CF_{mnw(t)} = ER_1(t) + ER_2(t) \tag{3}$$

Fig. 1b demonstrates the ability of incorporated energy ratios to enhance the presence of the first arrival onset, where it is shown that the new CF is greater in value and sharper than the traditional STA/LTA ratio at the first arrival time. Thereby, the accuracy in picking should be enhanced by comparing to traditional energy ratio methods.

Beside the drawbacks concerning windows size, threshold choice is another crucial problem of energy ratios methods (Akram and Eaton, 2012). We assume that the noise average does not depend on time, i.e. the seismic noise satisfies local stationary in short observation-scale (Ait Laasri et al., 2014). Consequently, when all windows are merely comprised of noise part, $ER_1$and ER_2 (given by **Eq.** (2) are circa one, resulting in CF_{mnw} around two (**Eq.** (3)). Based on these considerations, the theoretical threshold is given by **Eq.** (4):

$$Thr(t) = 2 + 3\sigma(t), \tag{4}$$

where $\sigma(t)$ is the standard deviation computed within the window preceding the instant t. By adding σ term in **Eq.** (4), the impact of most noise fluctuations should be mitigated, making this threshold slightly time dependent. However, when the later and delayed windows encompass a part of the seismic phases, the CF_{mnw} becomes greater than 2. The beginning of the potential zone (BPZ;

P-wavetrain trend) is determined once the CF_{mnw} exceeds *Thr(t)*. In order to minimize spike fluctuations on the picking procedure, a smoothing process of CF_{mnw} is performed via local regression tools (using for example *loess MatLab function*) within a window of half dominant period ($0.5\mathrm{T_d}$). Since CF_{mnw} characterizes the waveform change of the P-wavetrain, the potential first arrival times can be allocated to the two first local maxima of the smoothed CF_{mnw} (SCF_{mnw}) after BPZ within a predefined searching window. Therefore, one of the two initial picks that correspond to the maximum SNR represents the first break (tP_1) (**Fig. 1**). The approximated interval error (tE_1) can be assessed by $tE_1 = \max(e'_1, e''_1)$ where e'_1 is the absolute difference between BPZ and the first local maximum, and e''_1 is the absolute difference between the two maxima if they exist. The results of MNW method can be summarized by three parameters: the early beginning of the potential zone (*BPZ*), the potential first arrival time (tP_1), and the approximated interval error (tE_1).

Higher Order Statistics (HOS) method

The seismic noise follows closely a Gaussian probability distribution (Ait Laasri et al., 2014), while at the opposite, the seismic signal is non-Gaussian (Persson, 2003; Saragiotis et al., 2002). Higher statistics (as skewness and kurtosis which are normalized central moments of order three and four, respectively) are well suited to check the gaussianity of time series (Giannakis and Tsatsanis, 1994). Moving skewness and kurtosis reflect in different degrees the changes in distribution shape around a chosen position of the time series (Press et al., 1992). However, the ability of HOS to pick first arrivals was successfully tested by Saragiotis et al. (2002) for real seismic applications. Furthermore, the superior efficiency of kurtosis over other metrics (such as skewness) to detect and pick seismic phases has been shown by many authors (e.g. Küperkoch et al., 2010; Nippress et al., 2010).

In this study, kurtosis-based attribute (CF_k) was used to characterize the amplitude distribution, where CF_k is calculated using **Eq.** (5) with a n_k-samples moving window over the seismic trace.

$$CF_k(t) = \frac{1}{n_k} \sum_{i=t-n_k+1}^{t} \left(\frac{a_i - \overline{a_t}}{\sigma_t} \right)^4, \quad (5)$$

where a_i represents a vector of seismic amplitudes inside a window of size n_k , $\overline{a_t}$ and σ_t are respectively the mean and the standard deviation over n_k samples. The kurtosis-value for each window is ascribed to the end sample of the window (**Fig. 2**a). CF_k increases when the moving window integrates the first part of the seismic phase, due to the transition from Gaussian to non-Gaussian behavior (**Fig. 2**b). In case of complicated or emergent onsets, the kurtosis increases progressively before reaching its maximum value. The very beginning of this increase matches well the human-operator picking (Baillard et al., 2014). The onset time of the considered phase can be determined using the maximum CF_k derivative (Langet et al., 2014; Lois et al., 2013). To address this issue, we applied the successive transformations proposed by Baillard et al. (2014) to CF_k followed by smoothing; in a similar fashion as in MNW method, we can also apply low pass filtering to CF_k by using the same function and the smoothing parameters. Hence, the first arrival time (tP_2) is defined by the minimum of the smoothed Baillard's function (SCF_{Bk}) (**Fig. 2**b). We notice that when the non-impulsive arrivals are submerged by the noise, the kurtosis local maxima identifying this arrivals shift up in time. The approximated error (tE_2) can therefore be estimated by the time interval between the maximum of the CF_k function and the picked onset. For the clear and impulsive phases this time interval is very small, while in case of noisy and non-impulsive phases this interval becomes significantly larger. The results of HOS method can be summarized in two parameters: the potential first arrival time (tP_2) and the time sensibility range (tE_2).

Akaike Information Criterion (AIC) method

AIC (Akaike, 1974) is widely used in autoregressive (AR) techniques (e.g. Leonard and Kennett, 1999; Leonard, 2000; Takanami and Kitagawa, 1988). This approach is based on the assumption that the seismic trace can be split into locally stationary segments, where each of them is satisfying a different autoregressive model. Hence, the point where the AIC is minimized indicates the optimal separation of two time series (noise and signal plus noise) where the first break arrival (Sleeman and van Eck, 1999). In this study, instead of using AR coefficients for calculating AIC function, the CF based AIC (CF_{aic}) is calculated via Maeda's version (1985). Let $a(t)$ a seismic trace of length N, the CF_{aic} is computed by **Eq.** (6) directly from amplitudes sequences splitting in two segments (**Fig. 3**a).

$$CF_{aic}(t) = t\ log(\sigma^2(a)_{1\sim t}) + (N - t + 1)\, log(\sigma^2(a)_{t+1\sim N}), \quad (6)$$

where $\sigma^2(a)_{1\sim t}$ and $\sigma^2(a)_{t+1\sim N}$ are the variance of a in the backward and forward windows.

Under ideal conditions, the minimum of the CF_{aic} is searched for, and its corresponding time is interpreted as first arrival time. In some circumstances when noise and other later wavefield interfere, or when the seismic trace contains many significant features, AIC picker may fail to define the arrival as a global minimum. It is so necessary to apply AIC picker within a time limited window (*searching window*) containing only the useful phase (Zhang et al., 2003). Taking into account these points for improving the accuracy of AIC picking, we implemented the multi-model inference approach (Li et al., 2009). This approach incorporates the entire set of models in the searching window to compute a weighted average model, based on normalized Akaike weights as following:

- Define the minimum of the CF_{aic} in the searching window (CF_aic_{min}).
- Calculate the differences (Δ_i) between CF_{aic} values and CF_aic_{min}:

$$\Delta_i = CF_{aic_i} - CF\_aic_{min}, i = 1, \dots N \quad (7)$$

- Compute the normalized Akaike weights (AW):

$$AW_i = \frac{\exp(-\Delta_i/2)}{\sum_{r=1}^{N} \exp(-\Delta_r/2)} \quad (8)$$

- Set all values of (AW) out the searching window to zero.
- The potential first break time (tP_3) is obtained by using the weighted average:

$$tP_3 = \sum_{i=1}^{N} AW_i \; t_i, \quad (9)$$

where t_i is the time corresponding to each sample in the time series.

For traces showing high *SNR*, the difference between the improved AIC picker based on weighted model averaging scheme and ordinary AIC picker based on the best model (corresponding to the minimum AIC value) is negligible (**Fig. 3**b). On the other hand, when the traces show low *SNR* (where the global minimum of AIC function is not very sharp), the new AIC picker is more accurate since it integrates the other candidate models based on its relative importance estimated by Akaike weights (Li et al., 2009).

The sharpness of the AIC minimum often reflects the onset clarity (Diehl et al., 2009; Toomey et al., 1994). A prominent AIC minimum is typically produced by an impulsive event, whereas the broader local minima are related to non-impulsive or noisy events. We estimate the time uncertainty of AIC picker (tE_3) from normalized Akaike weights function within searching window. The lower and upper limit of error interval correspond with, respectively, to the first and last sample where AW is greater than an appropriate threshold. We found that a threshold of 10%

of the maximum AW function gives satisfying estimate of the uncertainty interval. The results of the AIC method can be summarized also by two parameters: the potential first-break of P-wave (tP_3), and the error range (tE_3).

However, in free-noisy traces one method is enough to pick correctly the first arrivals. Whereas in low SNR traces, each method picking has its own CF characterizing a specific property of the trace, their results may therefore be significantly different. Hence, using multi-method algorithm helps to fill gaps in each method maintaining a good performance, and further, to guide picking algorithm toward the interesting zone.

Algorithms implementation

The main idea of the implemented strategy is that multi-algorithm integration should enhance the picking capability of weak events and reduce picking errors whatever the noise level. In this three stage algorithm the information provided by each sub-algorithm is used either to orient the following phase picking (defining a target window), or to setup the essential parameters for the next phase, or both. The sequential integration of each sub-algorithm results in the implemented workflow provides auto adaptive parameter estimation. Therefore, one input parameter is needed only for the first picking algorithm (in MNW). Subsequently, all potential picks derived from sub-algorithms are used to determine the first arrival times and their corresponding relative errors. In the following subsections we describe the workflow of the complete picking algorithm and its parameters for a signal trace (trace-by-trace algorithm) and for a set of traces (entire-shot gather algorithm).

Single-trace algorithm picking

We extracted a vertical component seismic trace from a simulated record by finite differences modeling in order to describe the internal stage operations of the picking algorithm (input-output parameters and its respective CFs). A significant noise level (random and bandlimited noise) is added (

Fig. 4a). This trace presents a double serious challenge to be picked automatically, since the first arrival has a weak onset and is completely embedded within added noise. The first arrival was picked manually on clean trace before adding the noise and is marked by a black vertical solid line (

Fig. 4a).

Phase 1 (**MNW sub-algorithm**): the main goal of this phase is to enhance the presence of weak event and to determine the very beginning of the considering seismic phase. The CF characterizes the energy variations as a function of time. The first period length of the P-wave (T_d) is the only input parameter that needs fine-tune by the user. However, it can be obtained directly from the input data trace. For this test trace, we estimated T_d to 75 samples. The picking procedures, as described previously, are applied on the smoothed CF (SCF_{mnw}). The searching window (SW1) is located just after BPZ. We find a length equal to one and a half period ($1.5T_d$) is suited to pick the two local minima for which one of them is potentially the first arrival (tP_1).

Fig. 4b shows the SCF_{mnw} and the related results.

Phase 2 (**HOS sub-algorithm**): the size of the moving window (N_k) used in calculating the kurtosis-based (CF_K) can be estimated automatically from the approximated sensitivity

interval of the previous sub-algorithm (tE_1). For most tested traces, we found that N_k twice the (tE_1) provides satisfactory results. In order to avoid the under- or over-estimating of CF_K, we added a security condition in which when estimated N_k less than $0.5T_d$ or greater than $2T_d$, the algorithm setup the N_k to one period (T_d). The searching window ($SW2 = tE_1+T_d$) is automatically set up around the potential first arrival derived from MNW sub-algorithm (tP_1); tE_1 before tP_1 and T_d after. The potential first arrival (tP_2) and associated time uncertainty (tE_2) are also determined according to the descriptions in the related section (HOS method). The related CFs and results of this sub-algorithm are illustrated on the

Fig. 4c. It is worth mentioning that it is sufficient to compute the kurtosis attribute only for the part of the trace corresponding to the searching window, which speeds the picking process.

Phase 3 (**AIC sub-algorithm**): Since the performance of AIC methods depends strongly upon the searching window configuration, the results of previous sub-algorithms (MNW and HOS based kurtosis) were jointly used to lead the AIC picker, and further to setup its searching window size. We define the size of this window and its location (respectively, SW_3 *and* C_{aic}) according to **Eq.** (10).

$$SW_3 = 2\max(tE_1, tE_2)$$
$$C_{aic} = mean(tP_1, tP_2) \quad (10)$$

Finally, the potential first arrival (tP_3) and its time uncertainty (tE_3) are also obtained according to the related explications in AIC method section. The related attribute functions and the results are illustrated on the

Fig. 4d.

All potential first arrival onsets and their associated errors picked by the sub-algorithms are shown on the

Fig. 4e. The input/outputs parameters of each sub-algorithm can be summarized in the following simplified flows:

$$T_d\ (predefined\ by\ user) \xrightarrow{MNW\ sub-algo} BPZ, tP_1\ , and\ tE_1$$

$$tP_1\ and\ tE_1\ (from\ MNW\ sub-algo) \xrightarrow{HOS\ sub-algo} tP_2\ and\ tE_2$$

$$SW_3\ and\ C_{aic}\ \ (from\ MNW\ sub-algo\ \&\ HOS\ sub-algo) \xrightarrow{HOS\ AIC-algo} tP_3\ and\ tE_3$$

Final picking: In analogy to the multi-window and weighting scheme proposed by Lois et al. (2013), the final pick time (tP_{final}) is obtained by the weighted average of the picks set produced by the previous pickers ($tP_i; i = 1,2,3$) according to

$$tP_{final}\ = \frac{\sum_{i=1}^{3} Q_i\ tP_i}{\sum_{i=1}^{3} Q_i}, \tag{11}$$

where Q_i is a quality factor of the picked phase calculated into a predefined time windows and is given in dB (Küperkoch et al., 2010):

$$Q\ = 20\ log\left(\frac{A_s}{A_n}\right), \tag{12}$$

where A_n is the RMS-amplitude of the noise calculated within a time window of length ($nois\_wind = 3T_d$) before the determined tP_i. The A_s is the RMS-amplitude of the P-wave evaluated on the signal window ($sig\_wind = 1T_d$) starting immediately after tP_i.

In general, Q-values can yield crude information on the quality pick. If the arrival is correctly picked, Q has high and positive value. On the other hand, Q-value close to zero or negative indicates, respectively, very early picking (noise signal or dead trace) or late picking. All picks corresponding with negative Q values were excluded out the final picking process.

Error and quality assessment

While an ultimate goal of any automatic picker is to assure the highest accuracy possible, an associated uncertainty estimation is of great importance in *a posteriori* processing of first arrival time (*e.g.* in tomographic inversion). For these purposes, we suggest an approximated estimation of final pick error by using a simple statistical tool. From a practical and physical point view, the standard deviation can be considered as a good error estimator of repeated measurements of a physical parameter (here, the arrival time). Therefore, the final time uncertainty (tE_{final}) is produced by the standard deviation of three potential picks resulting from the aforementioned sub-algorithms.

$$tE_{final} = std(tP_1, tP_2, tP_3) \tag{13}$$

Since the first arrival onset is completely embedded by the random noise, the final pick is slightly shifted (

Fig. 4e). Therefore, that demonstrates the high sensibility of the three picking methods to the higher amplitudes. Although the considerable added noise, the correct first arrival time is still in the range error of the implement algorithm (

Fig. 4e).

Final picking reliability of single-trace algorithm:

To analyze the reliability of the final picking in the single-trace algorithm, we use a pseudo-synthetic dataset. These dataset was generated by adding 1000 noise scenarios to a real trace characterized by high SNR. Since the first-order Gauss-Markov process is the best candidate that can model the seismic noise (Baziw et al., 2004), we use this process to create the seed of our synthetic noise realizations as following:

- generation of a long time series (the seed series) of random noise via Gauss-Markov process.

- apply S-transform (Stockwell et al., 1996) on this one-dimensional noise.

- for each scenario, random selection (the bandlimited frequency and the start time) on the S-Transform time-frequency map , zeroing out of the selected zone and inverse S-Transform, normalization the output time series by its maximum and multiplication it by a random value (0.1 - 0.9).

The resultant noise scenarios can be considered more realistic in terms of random and bandlimited noises and S/N values. **Fig 5** illustrates the pseudo-synthetic dataset generation via one noisy trace realization.

The only input parameter (T_d) of the single-trace algorithm is about 30 ms. By assuming that the acceptable error is a quarter of the dominant period (T_d /4 = 7.5 ms), 70% of final picks falls in the interval error [-7.5, 7.5] with RMS value equal to 3.66 ms. A detailed view of the statistical analysis of the automatic picking results is shown in **Fig 6**. The time differences (automatic - manual) and final error normalized by T_d are shown as a function of first arrival quality (SNR) (**Fig 6a**), as well as their histogram distribution (**Fig 6b**). As expected, the algorithm performance deteriorates with

decreasing SNR. The quality of final picking and/or the normalized final error could be good criteria for assessing picked results. For this dataset, we can easily define 5 dB as a threshold for primary filtering out the bad picks with no good picks below this threshold. However, that is not evident for bad picks corresponds to earlier or later high amplitude produced by addition noise or posterior arrivals, respectively (**Fig 6d**).

To clarify the MNW effect on the final picking we perform a cross-analysis of MNW picking results. We define the acceptable error for MNW as $\pm T_d$. This error-value seems a reasonable choice because it corresponds to a part of the searching window of HOS that follows the initial pick estimates from MNW. **Fig 6c** shows time difference pie chart for the four possible cross-combinations of MNW and Final Picking (FP) results. Among 70% of successful FP in its interval error, only 2% of picks were not initialized by MNW. Otherwise, despite than 9% of picks were well initialized by the MNW algorithm, the FP could not pick them correctly due to the relative high-quality weighting of the other pickers (HOS and AIC). Most of these picks are often associated with later arrivals. The MNW could not determine the potential zone of the last 21%. Since energy ratio algorithms are sensitive to high noise fluctuations (Akram and Eaton, 2016a), MNW was probably trapped by high-amplitude noise fluctuations far from the first arrival. The same behavior is observed for FP. The corresponding picks are characterized by low final quality picking (**Fig 6d**).

Normalizing the pick quality by the corresponding errors issued from final picking can be considered as a good criterion to evaluate the three stage algorithm consistency. High values indicate a good arrival quality, and the sub-algorithms will therefore pick in a narrow time interval (small error), whereas lower values (close to 0) correspond to erroneous first arrival (noise) or/and

dispersive picks algorithms (large error). **Fig 7** shows the consistence of three algorithms on the categories in the **Fig 6**.

A drawback of the three-stage algorithm occurs when the MNW stage fails to successfully define the BPZ, leading to sequential failure as sub-algorithms are inter-connected by auto adaptive parameters transmission, and to false picking. In such case, high-fidelity filtering (e.g. Aldersons, 2004) or denoising (e.g. Parolai, 2009; Tselentis et al., 2012; Gaci, 2014) are still possible during pre-processing. In near surface seismic surveys, exploitation of multi-trace redundant data and events coherency is another candidate solution.

Entire-shot record algorithm picking

The basic idea of this algorithm is to integrate all picks provided from preceding sub-algorithms by exploitation the properties of coherency of the first arrivals and its consistency over all offsets. This algorithm is an extension of the single-trace algorithm, and it is adapted for full automatically picking of common shot-gathers. In order to better determine the trend of P-wavetrain and to work under different noise conditions we optimized MNW sub-algorithm by adding/involving two tools; variable-threshold engine and look-like Monte Carlo approach.

Using a fixed MNW-threshold might lead to false picking due to the high variability of the noise and the P-waveforms. In order to elevate this drawback, we proposed a variable-threshold engine combined with an iterative process. The latter is a look-like Monte Carlo approach; an optimal solution is built from the database picks that arise from MNW sub-algorithm via variable thresholding. Here, the solution is the set of picks (BPZ picks) forming the first-breaks trend over the whole shot gather. Using two subroutines: In the first one, a matrix of all possible solutions is generated by a multi threshold engine picking (the threshold varies between 0.5 and 10). The second

one is an iterative system consisting of: (1) randomly building a solution, (2) calculating the corresponding cost function, (3) repeating the process for a predetermined number of iterations, (4) choosing the best solution which corresponds to maximum of the cost function. Our cost function combines three main properties in order to highlight the presence of the first arrivals:

Energy cost function ($Cost_{En}$): we defined $Cost_{En}$ (**Eq.** (14)) as a function of the after-energy ratio (AER) modulated by given picks quality (Q) and normalized by an error ($Error_{ER}$). AER is CF_{mnw} average within a limited window just after the built solution. Q is estimated by **Eq.** (12). $Error_{ER}$ is given by the standard deviation of the solutions matrix over threshold dimension ($Std_{\ gr}$). This cost function has to maximize over the whole shot record.

$$Cost_{En} = \sum \left(\frac{AER \times Q}{2\ Error_{ER}} \right)^2 \qquad (14)$$

$$Error_{ER} = Std_{\ gr}$$

Smooth cost function ($Cost_{smooth}$): by definition, a curve is smooth when all the derivatives exist and are continuous. The simplicity and efficiency of centered second-order derivative ($deriv2$) make it an attractive candidate for analyzing smoothness curve. The second order derivative of the travel time shape has to minimize (*i.e.* the solution is hold as close as possible to a smooth curve). The shape of the trend is normalized by an attributed error ($Error_{smooth}$), which can be defined as the standard deviation of the selected solution (Std_{sol}). The $Cost_{smooth}$ is then given through the **Eq.** (15):

$$Cost_{smooth} = \sum \left(\frac{|deriv2|}{2\ Error_{smooth}} \right)^2$$
$$Error_{smooth} = Std_{sol}\,. \tag{15}$$

SNR cost function ($Cost_{snr}$): the $Cost_{snr}$ is defined by **Eq.** (16), and has to be maximized.

$$Cost_{snr} = \sum \left(\frac{Snr}{2\ Error_{snr}} \right)^2$$
$$Error_{snr} = Std_{gr} + Std_{sol}, \tag{16}$$

where Snr is calculated for raw traces in predetermined windows around the built solution.

The total cost function is the sum of the normalized costs functions as follows:

$$Cost_{total} = \alpha \cdot Cost_{En} + \frac{\beta}{Cost_{smooth}} + \gamma \cdot Cost_{snr}, \tag{17}$$

where α, β and γ are weights in [0, 1], which allow controlling the importance of individual objective functions. In this study, we give an equal contribution of the three cost functions ($\alpha = \beta = \gamma = 1$). The trend of the first arrivals is then to find the optimal solution (sol^*) which maximize the total cost function ($Cost_{total}$). The problem can be simply formulated as,

$$sol^* = arg \max_{sol} Cost_{total} \tag{18}$$

The general flow of our iterative system is somewhat similar to Monte Carlo approach (randomizing selection and then minimizing a likelihood function). In our approach, the random selection is limited or somehow guided, and the likelihood function is absent (i.e. full directly searching).

Taking in consideration that the first arrivals are consistent and coherent over all offsets, their trend should be as smoothed as possible. In order to eliminate outliers and high first order derivative points, the final solution should be passed through a smoothing process. We used *rloess matlab* function, which is based on local regression using linear least squares; it assigns lower weights to outliers during the regression. The smoothing window length is chosen depending on the complexity of subsurface and therefore on the expected form of travel time curve (in percent of total traces number).

In very noisy case, the correct first arrivals could be found in the shadow of strong ambient noise. Hence, they might be invisible for the variable-threshold engine. In such case, it is preferred to rebuild the solutions matrix, but within a small tolerance window centered on the smoothed solution. The tolerance window length of two time dominant period ($2T_d$) is suitable for this purpose. The new candidate matrix is processed again though the iterative system. The final smoothed solution can then be interpreted as the trend of the potential zone of the P-wavetrain arrivals.

As a whole, the rest of the algorithm has the same workflow as the single-trace algorithm. In particular, the input parameters of each sub-algorithm (especially the searching windows size) were adjusted by using statistical tools. The abundance of each sub-algorithm outputs permits also to set forwardly the SW location for the next sub-algorithm (i.e. guiding mode).

Since the trend might be delayed due to use of multi-threshold and/or smoothing process in MWN sub-algorithm, it is appropriate to add a confidence interval ($0.5\ T_d$) before the estimating smoothed trend. Therefore, the P-wavetrain zone is located around the smoothed trend rather than just after it (as in single-trace algorithm).

The parameters setting of all sub-algorithms are recapitulated in the

Table 1 that presents a comparative summary of the two algorithms' parameters.

VALIDATION THE PROPOSED ALGORITHM

Test on synthetic data

Synthetic datasets were produced by finite-difference (FD) modelling in the time-space domain using *FDELMODC* program developed by Thorbecke and Draganov (2011). The geometry of the acquisition system consists of an array of 72 receivers with a spacing of 4 m in flat topography. The seismic sources are simulated by an explosive Ricker wavelet with maximum-frequency of 90 Hz, spreading every 4 m between the receivers. The geological model used to create wavefield data is assumed to be an elastic media incorporating realistic subsurface structures. This model is composed of many layers (C1-C3) and a substratum (S) fractured by a normal fault (F); three layers at the left side of the fault and two layers on the right one (**Fig. 8**a). All velocities and densities are assumed to be constant in each layer, except the fault zone with a linear velocity gradient about 12.5 m/s per m, with v_0 = 625 m/s. Densities (ρ) are set using the Grardner's rule for P-wave velocities ($\rho = 0.31V_p^{0.25}, V_p\ in\ m/s\ and\ \rho\ in\ g/cm^3$) for each layer. The details about the model geometrical parameters are shown in **Fig. 8**a and

Table 2. Since FD modelling requires to grid the model into a finite number of cells (Carcione et al., 2002), the model (500 x 150 m) was discretized into 1000 x 300 grid mesh (i.e. the space is equally sampled in x and z at 0.5 m). The Perfected Matched Layer (PML) absorbing boundary with 120 grid points was implemented along at three sides, with free surface. We generate many inline shot gathers; in each one, a total of 0.6 s with time increment of 0.5 ms was modelled for the vertical point force located at the free surface. **Fig. 8**b shows an example end-on spread shot-gather (the source at 198 m) of the vertical component of the wavefield simulated, in which the theoretical P-wave arrival times are denoted in small green circles.

We added the noise adding to the simulated wavefields, which represents another difficulty inherent to weak events, along complex changes in the waveforms, and nonlinear travel-time curve in presence of a fault. Two types of added noise (random zero-mean Gaussian and band-limited noises) were computed using the function *suaddnoise* of the Seismic Unix (SU) package (Cohen and Stockwell, 2012). The band-limited noise has approximately the double frequency range of the simulated source.

We applied the entire-shot picking algorithm to pick the first arrival times in the shot gather shown in **Fig. 8**b Jan Kroon under an open source license (https://fr.mathworks.com/matlabcentral/fileexchange/24531-accurate-fast-marching, last accessed March 1st, 2018). The automatic process was repeated for the same shot-gather in **Fig. 8a** but with additive random Gaussian noise of 20%, with limited-band noise by [40-180] Hz, followed by the two previous noises together (**Fig. 8**b, **Fig. 8**c, and **Fig. 8**d), respectively. The picks resulting from the automatic algorithm have a good overall consistence with the theoretical picks. Although automatic picking performed satisfactorily, an over-estimating of the arrival times is noticed after adding the

noise. This shift-down of the picks increases with the offset and it is remarkable at the events corresponding to the fault.

To assess our algorithm robustness, we compare the picks with those determined theoretically for two cases: noise-free and noisy records. In the case of noise-free shot gather, 60% of the automatic picks are within [0,-2] ms of the actual picks, and 90% are within [0, -10] ms (**Fig. 9**a, red histogram). This analysis can be considered as a calibration step of the algorithm parameter setting; the median value of the automatic-manual differences is about -1 ms. A possible explanation of this deviation is that the P-wave dominant period length varies with the offset. For noisy data (random and band-limited noises), the blue histogram in **Fig. 9a** shows that about 35% of the differences are found at 10 ms, and 75% are within [0, 20] ms. **Fig. 9**b shows a statistical analysis per quality class, which are determined in analogy to the empirical uncertainty categories (A-D) of Lois et al. (2013). Clearly, all distributions of the four classes are found on the positive side of the difference between automatic and actual picks. The visual check of individual sub-algorithm results and corresponding waveforms shows that delay time picking is mainly due to their high sensibility to the high amplitudes in the presence of high noise levels. The dispersion symmetry around the median and the absence of outliers show again good consistence of the two picking methods.

With noise addition, the first arrivals quality was degraded by about 20% of their level at the noise-free gather (**Fig. 10**; see red dotted curves evaluation comparing to the red solid ones). The accuracy of our adaptive algorithm versus the first arrivals quality is presented in the tables included in the **Fig. 10**. The Root-Mean-Square (RMS) of the differences in case of zero noise is 3.6 ms, and the maximum RMS in noisy cases is 16 ms, which normally corresponds with C and D quality classes. Generally, increased noise levels result in anomalously late picks, because parts or even complete

phases of the recorded signal can be masked by the noise. The implemented algorithm kept a good performance despite the decreasing of quality arrival due to additive noise, where the maximum RMS in the very noisy case did not exceed the acceptable error.

Test on real data

Exploration-scale active-source seismic dataset was chosen to validate the implemented algorithm on real data. The dataset is characterized by a variable quality level of first arrivals when increasing source-receiver distances. The performance assessment is achieved by comparing the algorithm result with those manually picked. The Douglas's concept (1997) “the less filtering, the better picking algorithm” has been applied, where no data preprocessing was performed before the automatic picking process, but all traces are scaled with respect to their maximum value.

Field data

As a test, we have applied our algorithm to a 800-m-long seismic profile conducted in the Chaux Forest in the Jura region (France). An accelerated 40 kg weight (hitch-mounted at the front of a tractor) dropped onto a steel plate, is used as a seismic source for generating the energy, with 4 m source interval along the profile. Four shots at each source location were averaged to increase the signal-to-noise ratio. The recorder system consists of 72 14-Hz vertical component geophones, with 4 m receiver spacing along 318 m of maximum offset. The recording time was 1 s with a delay of -20 ms. The data were sampled at 1 ms. A roll-along technique acquisition was used to perform the total profile survey. In this study more than 12500 recorded traces were considered from 174 shots.

The dominant period (T_d) of the P-waves can be directly estimated by visual inspection of the seismic section. Since the earth acts as a minimum phase low pass filter (Aki and Richards, 1980), T_d

tends to become larger at far-offsets. Following the initial inspections on individual shot gathers, six periods ranging from 11 to 35 samples in length were examined. This key parameter was calibrated through a trial-and-error procedure in order to unify its value over all offsets. We can see that a value of 25 samples is a reasonable choice because it provides the best compromise between minimum RMS and maximum traces picked within the predefined margin error of manual picking (±5 ms) (**Fig. 11**). This error-value corresponds to approximately a quarter period of the 40–50 Hz first arrival signals (Zelt et al., 2006). The other required parameters are set up automatically during the process (i.e. auto adaptive parameters) as described in the previous sections.

In order to reduce calculation time, only the first 250 ms of the time record were taken in consideration. **Fig. 12** shows an example of the picking results by our adaptive algorithm (blue line) with related error, and those picked manually (green line). Unlike the far-offset traces, an excellent agreement is observed between manual and automatic picks of near-offset traces.

Applying the proposed algorithm to the whole profile data (more than 12500 traces), more than 88% of traces were picked in the implicit presumed error interval of the manual picks (±5 ms), with only 7 ms as RMS. A more detailed view of the statistical analysis of the automatic picking results is shown in **Fig. 13**. The residuals between our automatic picks and manual picks (automatic-manual) are shown as a function of offset (**Fig. 13a**) and first arrivals quality (SNR) (**Fig. 13b**), as well as their distribution in a histogram (**Fig. 13c**). The residuals decrease quickly and concentrate (close to zero) for the high quality traces, which largely reflect the high performance of the proposed algorithm. Unfortunately, the residuals depart from zero after offset 200 m and are dispersed in the positive side, which suggests that our algorithm picks systematically late arrivals at far-offsets. Another possible explanation of this deviation is that the increasing dominant period length with

offset might have a significant effect on algorithm accuracy. The signal-to-noise ratio (SNR) is however the main source of error for even a manual picking (Zeiler and Velasco, 2009). **Fig. 13d** shows the normalized cumulative histogram of the related picking errors, with 90% of the available traces picked with standard errors less than ±3 ms.

However, the tendency of late picking at those offsets reinforces the need to enhance these arrivals before automatic picking, or at least to omit automatically or manually their picks before any posterior processing. Additionally, there might be some dead traces where their picks are naturally wrong and must be also ignored (Sabbione and Velis, 2010).

A further advantage of the proposed algorithm is that the individual error derived automatically can be employed to define the pick quality, thus weighting the data in travel time inversion (e.g. Bauer et al., 2010). Furthermore, the performance of the developed algorithm versus other automatic pickers and with many datasets recorded by various sources-types was stated by Khalaf (2016).

From our experience, the new algorithm processes 72 traces shot gather in about 10 seconds along with thorough quality check. Since this study is primarily focused on accurate picking, no attention is paid to time calculation improvement that may be a subject of further research.

CONCLUSIONS

We have introduced an adaptive multi-method algorithm to pick automatically the first arrival times of near surface seismic data by combining three methods (MNW, HOS, and AIC). The MNW method was combined with iterative look-like Monte Carlo approach supplying a good localization of the first arrivals trend, even if the arrival onset embedded by a high noise level.

Integrating the three methods results as a combination of the first arrival properties (energy, gaussianity, and stationarity) yielded fruitfully as a precise, nearly parameter-free, and full automatic picking algorithm.

Testing our algorithm on synthetic and real data demonstrated good results in comparison to those calculated theoretically and picked manually, respectively. The synthetic example presented in this paper is realistic for near-surface studies in terms of the velocities distribution, depth investigation, source–receiver geometries, and noise data. The noise robustness tests (with no added noise and with additive random Gaussian and limited-band noises) demonstrated the overall reliability of proposed algorithm, resulting in maximum RMS of 16 ms in the case of exaggerated noise. For real data, the effectiveness of the proposed picking method is highly dependent on the quality of the first arrivals and their dominant period, which is the key parameter in the overall methodology.

The proposed algorithm provides automatically not only the first arrival times, but also their uncertainties. These uncertainties can be used in *a posteriori* processing such as in tomographic inversion or data phase-editing prior inversion.

The number of user-tuning parameters was kept as low as possible as in order to reduce parameters errors. In fact, the main period of the first arrivals is the only required parameter. All the others parameters are auto-estimated and adapted across the processing workflow.

Finally, in cases of very weak events with high noise presence, local enhancement of the first arrival signals may help to improve our algorithm accuracy. For instance, like this enhancement may be achieved by local stacking or very high fidelity denoising. Our algorithm is appropriate for

common shot gather, but it is expected to provide a basis for more effective picking on other seismic data collections, such as common-offset gather (COG). However, their detailed advantages and drawbacks analysis is beyond the scope of the present paper.

ACKNOWLEDGEMENTS AND DATA

The synthetic data will be available for download upon request. The authors are grateful to Dr. Antoine Chevalier for a number of helpful comments and suggestions concerning to Monte Carlo approach, and to Dr. Sylvain Pasquet, Dr. Mustafa Senkaya and another anonymous reviewer for their very constructive comments, which helped to significantly improve the present manuscript.

REFERENCES

Ait Laasri, E.H., Akhouayri, E.S., Agliz, D., Atmani, A., 2014. Automatic detection and picking of P-wave arrival in locally stationary noise using cross-correlation. Digit. Signal Process. A Rev. J. 26, 87–100. doi:10.1016/j.dsp.2013.12.009

Akaike, H., 1974. Markovian representation of stochastic processes and its application to the analysis of autoregressive moving average processes. Ann. Inst. Stat. Math. 26, 363–387. doi:10.1007/BF02479833

Akaike, H., 1971. Autoregressive model fitting for control. Ann. Inst. Stat. Math. 23, 163–180. doi:10.1007/BF02479221

Aki, K., Richards, P.G., 1980. Quantitative seismology. W.H. Freeman and Company.

Akram, J., Eaton, D., 2012. Adaptive microseismic event detection and automatic time picking, in: GeoConvention 2012. pp. 1–5.

Akram, J., Eaton, D.W., 2016a. A review and appraisal of arrival-time picking methods for downhole

microseismic data. GEOPHYSICS 81, KS71-KS91. doi:10.1190/geo2014-0500.1

Akram, J., Eaton, D.W., 2016b. Refinement of arrival-time picks using a cross-correlation based workflow. J. Appl. Geophys. 135, 55–66. doi:10.1016/j.jappgeo.2016.09.024

Aldersons, F., 2004. Toward a Three-Dimensional Crustal Structure of the Dead Sea region from Local Earthquake Tomography. PhD thesis. Tel-Aviv University.

Allam, A.A., Ben-Zion, Y., Peng, Z., 2014. Seismic Imaging of a Bimaterial Interface Along the Hayward Fault, CA, with Fault Zone Head Waves and Direct P Arrivals. Pure Appl. Geophys. 171, 2993–3011. doi:10.1007/s00024-014-0784-0

Allen, R., 1982. Automatic phase pickers: Their present use and future prospects. Bull. Seismol. Soc. Am. 72, S225-242.

Allen, R., 1978. Automatic earthquake recognition and timing from single traces. Bull. Seismol. Soc. Am. 68, 1521–1532.

Anant, K.S., Dowla, F.U., 1997. Wavelet transform methods for phase identification in three-component seismograms. Bull. Seismol. Soc. Am. 87, 1598–1612.

Baer, M., Kradolfer, U., 1987. An automatic phase picker for local and teleseismic events. Bull. Seismol. Soc. Am. 77, 1437–1445.

Baillard, C., Crawford, W.C., Ballu, V., Hibert, C., Mangeney, A., 2014. An Automatic Kurtosis-Based P- and S-Phase Picker Designed for Local Seismic Networks. Bull. Seismol. Soc. Am. 104, 394–409. doi:10.1785/0120120347

Bauer, K., Moeck, I., Norden, B., Schulze, A., Weber, M., Wirth, H., 2010. Tomographic P wave velocity and vertical velocity gradient structure across the geothermal site Groß Schönebeck (NE German Basin): Relationship to lithology, salt tectonics, and thermal regime. J. Geophys.

Res. 115, 1–22. doi:10.1029/2009JB006895

Baziw, E., Nedilko, B., Weir-Jones, I., 2004. Microseismic Event Detection Kalman Filter: Derivation of the Noise Covariance Matrix and Automated First Break Determination for Accurate Source Location Estimation. Pure Appl. Geophys. 161, 303–329. doi:10.1007/s00024-003-2443-8

Billings, S.D., Sambridge, M.S., Kennett, B.L.N., 1994. Errors in hypocenter location: Picking, model, and magnitude dependence. Bull. Seismol. Soc. Am. 84, 1978–1990.

Blias, E., 2012. Optimization approach to automatic first arrival picking for three-component three-dimensional vertical seismic profiling data. Geophys. Prospect. 60, 1024–1029. doi:10.1111/j.1365-2478.2011.01014.x

Bogiatzis, P., Ishii, M., 2015. Continuous Wavelet Decomposition Algorithms for Automatic Detection of Compressional- and Shear-Wave Arrival Times. Bull. Seismol. Soc. Am. 105, 1628–1641. doi:10.1785/0120140267

Carcione, J.M., Herman, G.C., ten Kroode, A.P.E., 2002. Seismic modeling. Geophysics 67, 1304–1325. doi:10.1190/1.1500393

Chen, Z., 2005. A multi-window algorithm for automatic picking of microseismic events on 3-C data, in: SEG Technical Program Expanded Abstracts 2005. Society of Exploration Geophysicists, pp. 1288–1291. doi:10.1190/1.2147921

Cichowicz, A., 1993. An automatic S-phase picker. Bull. Seismol. Soc. Am. 83, 180–189.

Cohen, J.K., Stockwell, J.J.W., 2012. CWP/SU: Seismic Un*x Release No. 43R1: an open source software package for seismic research and processing. Cent. Wave Phenomena, Color. Sch. Mines.

Coppens, F., 1985. First arrival picking on common-offset trace collections for automatic estimation

of static corrections. Geophys. Prospect. 33, 1212–1231. doi:10.1111/j.1365-2478.1985.tb01360.x

Di Stefano, R., Aldersons, F., Kissling, E., Baccheschi, P., Chiarabba, C., Giardini, D., 2006. Automatic seismic phase picking and consistent observation error assessment: application to the Italian seismicity. Geophys. J. Int. 165, 121–134. doi:10.1111/j.1365-246X.2005.02799.x

Diehl, T., Deichmann, N., Kissling, E., Husen, S., 2009. Automatic S-wave picker for local earthquake tomography. Bull. Seismol. Soc. Am. 99, 1906–1920. doi:10.1785/0120080019

Douglas, A., 1997. Bandpass filtering to reduce noise on seismograms: Is there a better way? Bull. Seismol. Soc. Am. 87, 770–777.

Earle, P.S., Shearer, P.M., 1994. Characterization of Global Seismograms Using an Automatic-Picking Algorithm. Bull. Seismol. Soc. Am. 84, 366–376.

Gaci, S., 2014. The use of wavelet-based denoising techniques to enhance the first-arrival picking on seismic traces. IEEE Trans. Geosci. Remote Sens. 52, 4558–4563. doi:10.1109/TGRS.2013.2282422

Gelchinsky, B., Shtivelman, V., 1983. Automatic picking of first arrivals and parameterization of traveltime curves*. Geophys. Prospect. 31, 915–928. doi:10.1111/j.1365-2478.1983.tb01097.x

Geoltrain, S., Brac, J., 1993. Can we image complex structures with first-arrival traveltime? Geophysics 58, 564–575. doi:10.1190/1.1443439

Giannakis, G.B., Tsatsanis, M.K., 1994. Time-domain tests for Gaussianity and time-reversibility. IEEE Trans. Signal Process. 42, 3460–3472. doi:10.1109/78.340780

Hafez, A.G., Khan, T.A., Kohda, T., 2009. Earthquake onset detection using spectro-ratio on multi-threshold time-frequency sub-band. Digit. Signal Process. A Rev. J. 19, 118–126.

Han, L., Wong, J., Bancroft, J., 2009. Time picking and random noise reduction on microseismic data: CREWES Research Report.

Hatherly, P.J., 1982. A computer method for determining seismic first arrival times. Geophysics 47, 1431–1436. doi:10.1190/1.1441291

Iqbal, N., Al-Shuhail, A.A., Kaka, S.L.I., Liu, E., Raj, A.G., McClellan, J.H., 2017. Iterative interferometry-based method for picking microseismic events. J. Appl. Geophys. 140, 52–61. doi:10.1016/j.jappgeo.2017.03.005

Jiao, L., Moon, W.M., 2000. Detection of seismic refraction signals using a variance fractal dimension technique. Geophysics 65, 286–292. doi:10.1190/1.1444719

Khalaf, A., 2016. Développement d'une nouvelle technique de pointé automatique pour les données de sismique réfraction. Université Pierre et Marie Curie - Paris VI.

Küperkoch, L., Meier, T., Brüstle, A., Lee, J., Friederich, W., 2012. Automated determination of S-phase arrival times using autoregressive prediction: application to local and regional distances. Geophys. J. Int. 188, 687–702. doi:10.1111/j.1365-246X.2011.05292.x

Küperkoch, L., Meier, T., Lee, J., Friederich, W., Working Group, E., 2010. Automated determination of P -phase arrival times at regional and local distances using higher order statistics. Geophys. J. Int. 181, 1159–1170. doi:10.1111/j.1365-246X.2010.04570.x

Langet, N., Maggi, A., Michelini, A., Brenguier, F., 2014. Continuous Kurtosis-Based Migration for Seismic Event Detection and Location, with Application to Piton de la Fournaise Volcano, La Reunion. Bull. Seismol. Soc. Am. 104, 229–246. doi:10.1785/0120130107

Lanz, E., Maurer, H., Green, A., 1998. Refraction tomography over a buried waste disposal site. Geophysics 63, 1414–1433. doi:10.1190/1.1444443

Lawton, D.C., 1989. Computation of refraction static corrections using first-break traveltime differences. Geophysics 54, 1289–1296. doi:10.1190/1.1442588

Leonard, M., 2000. Comparison of Manual and Automatic Onset Time Picking. Bull. Seismol. Soc. Am. 90, 1384–1390. doi:10.1785/0120000026

Leonard, M., Kennett, B.L.N., 1999. Multi-component autoregressive techniques for the analysis of seismograms. Phys. Earth Planet. Inter. 113, 247–263. doi:10.1016/S0031-9201(99)00054-0

Li, C., Huang, L., Duric, N., Zhang, H., Rowe, C., 2009. An improved automatic time-of-flight picker for medical ultrasound tomography. Ultrasonics 49, 61–72. doi:10.1016/j.ultras.2008.05.005

Lois, A., Sokos, E., Martakis, N., Paraskevopoulos, P., Tselentis, G.-A., 2013. A new automatic S-onset detection technique: Application in local earthquake data. Geophysics 78, KS1-KS11. doi:10.1190/geo2012-0050.1

Lomax, A., Satriano, C., Vassallo, M., 2012. Automatic Picker Developments and Optimization: FilterPicker--a Robust, Broadband Picker for Real-Time Seismic Monitoring and Earthquake Early Warning. Seismol. Res. Lett. 83, 531–540. doi:10.1785/gssrl.83.3.531

Lou, X., van der Lee, S., Lloyd, S., 2013. AIMBAT: A Python/Matplotlib Tool for Measuring Teleseismic Arrival Times. Seismol. Res. Lett. 84, 85–93. doi:10.1785/0220120033

Maeda, N., 1985. A method for reading and checking phase times in auto-processing system of seismic wave data. Zisin = Jishin 38, 365–380.

Mallinson, I., Bharadwaj, P., Schuster, G., Jakubowicz, H., 2011. Enhanced refractor imaging by supervirtual interferometry. Lead. Edge 30, 546–550. doi:10.1190/1.3589113

Mousa, W.A., Al-Shuhail, A.A., 2012. Enhancement of first arrivals using the τ-p transform on energy-ratio seismic shot records. Geophysics 77, V101–V111. doi:10.1190/geo2010-0331.1

Mousa, W.A., Al-Shuhail, A.A., Al-Lehyani, A., 2011. A new technique for first-arrival picking of refracted seismic data based on digital image segmentation. Geophysics 76, V79–V89. doi:10.1190/geo2010-0322.1

Nippress, S.E.J., Rietbrock, A., Heath, a. E., 2010. Optimized automatic pickers: application to the ANCORP data set. Geophys. J. Int. 181, 911–925. doi:10.1111/j.1365-246X.2010.04531.x

Parolai, S., 2009. Denoising of Seismograms Using the S Transform. Bull. Seismol. Soc. Am. 99, 226–234. doi:10.1785/0120080001

Pavlis, G.L., Vernon, F.L., 2010. Array processing of teleseismic body waves with the USArray. Comput. Geosci. 36, 910–920. doi:10.1016/j.cageo.2009.10.008

Peraldi, R., Clement, A., 1972. Digital processing of refraction data study of first arrivals*. Geophys. Prospect. 20, 529–548. doi:10.1111/j.1365-2478.1972.tb00653.x

Persson, L., 2003. Statistical tests for regional seismic phase characterizations. J. Seismol. 7, 19–33. doi:10.1023/A:1021216313892

Press, W.H., Teukolsky, S.A., Vetterling, W.T., Flannery, B.P., 1992. Numerical recipes in C : the art of scientific computing, Second Edi. ed. doi:10.1016/0898-1221(90)90201-T

Ramananantoandro, R., Bernitsas, N., 1987. A computer algorithm for automatic picking of refraction first-arrival time. Geoexploration 24, 147–151. doi:10.1016/0016-7142(87)90088-3

Ricker, N., 1953. The form and laws of propagation of seismic wavelets. Geophysics 18, 10–40. doi:10.1190/1.1437843

Ross, Z.E., Ben-Zion, Y., 2014. Automatic picking of direct P, S seismic phases and fault zone head waves. Geophys. J. Int. 199, 368–381. doi:10.1093/gji/ggu267

Sabbione, J.I., Velis, D., 2010. Automatic first-breaks picking: New strategies and algorithms.

Geophysics 75, V67–V76. doi:10.1190/1.3463703

Saragiotis, C.D., Hadjileontiadis, L.J., Panas, S.M., 2002. PAI-S/K: A robust automatic seismic P phase arrival identification scheme. IEEE Trans. Geosci. Remote Sens. 40, 1395–1404. doi:10.1109/TGRS.2002.800438

Saragiotis, C.D., Hadjileontiadis, L.J., Rekanos, I.T., Panas, S.M., 2004. Automatic P Phase Picking Using Maximum Kurtosis and k-Statistics Criteria. IEEE Geosci. Remote Sens. Lett. 1, 147–151. doi:10.1109/LGRS.2004.828915

Senkaya, M., Karslı, H., 2014. A semi-automatic approach to identify first arrival time: the Cross-Correlation Technique. Earth Sci. Res. J. 18, 107–113. doi:10.15446/esrj.v18n2.35887

Sleeman, R., van Eck, T., 1999. Robust automatic P-phase picking: an on-line implementation in the analysis of broadband seismogram recordings. Phys. Earth Planet. Inter. 113, 265–275. doi:10.1016/S0031-9201(99)00007-2

Stewart, W.S., 1977. Real-time detection and location of local seismic events in central california. Bull. Seismol. Soc. Am. 67, 433–452.

Stockwell, R., Mansinha, L., Lowe, R.P., 1996. Localization of the complex spectrum: the S transform. Signal Process. IEEE Trans. 44, 998–1001. doi:10.1109/78.492555

Takanami, T., Kitagawa, G., 1988. A new efficient procedure for the estimation of onset times of seismic waves. J. Phys. Earth 36, 267–290. doi:10.4294/jpe1952.36.267

Thorbecke, J.W., Draganov, D., 2011. Finite-difference modeling experiments for seismic interferometry. Geophysics 76, H1–H18. doi:10.1190/geo2010-0039.1

Toomey, D.R., Solomon, S.C., Purdy, G.M., 1994. Tomographic imaging of the shallow crustal structure of the East Pacific Rise at 9°30'N. J. Geophys. Res. 99, 24135–24157.

doi:10.1029/94JB01942

Trnkoczy, A., 2012. Understanding and parameter setting of STA / LTA trigger algorithm 1 Introduction. New Man. Seismol. Obs. Pract. 2 2, 1–20. doi:10.23 12/GFZ.NMSOP - 2 _IS_8.1

Tselentis, G.-A., Martakis, N., Paraskevopoulos, P., Lois, A., Sokos, E., 2012. Strategy for automated analysis of passive microseismic data based on S-transform, Otsu's thresholding, and higher order statistics. Geophysics 77, KS43-KS54. doi:10.1190/geo2011-0301.1

VanDecar, J., Crosson, R., 1990. Determination of teleseismic relative phase arrival times using multi-channel cross-correlation and least squares. Bull. Seismol. Soc. Am. 80, 150–169.

Wong, J., Han, L., Bancroft, J.C., Stewart, R., 2009. Automatic time-picking of first arrivals on noisy microseismic data, in: CSEG. CREWES, pp. 1–6.

Yilmaz, Ö., 2001. Seismic data analysis: Processing, Inversion, and Interpretation of Seismic Data (Investigations in Geophysics, No. 10), 2nd Editio. ed. Society of Exploration Geophysicists.

Zeiler, C., Velasco, A.A., 2009. Seismogram Picking Error from Analyst Review (SPEAR): Single-Analyst and Institution Analysis. Bull. Seismol. Soc. Am. 99, 2759–2770. doi:10.1785/0120080131

Zelt, C.A., Azaria, A., Levander, A., 2006. 3D seismic refraction traveltime tomography at a groundwater contamination site. Geophysics 71, H67–H78.

Zelt, C.A., Drew, J.J., Yedlin, M.J., Ellis, R.M., 1987. Picking noisy refraction data using semblance supplemented by a Monte Carlo procedure and spectral balancing. Bull. Seismol. Soc. Am. 77, 942–957.

Zhang, H., Thurber, C., Rowe, C., 2003. Automatic P -Wave Arrival Detection and Picking with Multiscale Wavelet Analysis for Single-Component Recordings. Bull. Seismol. Soc. Am. 93, 1904–1912. doi:10.1785/0120020241

List of captions

Tables

Figures

Table 1 : Comparative summary of the modification between the single-trace and entire-shot algorithms parameters (~: no parameters, ==: the same parameters).

	Single-trace Algorithm			Entire-shot Algorithm		
	Sub-algorithms			Sub-algorithms		
Parameters	**MNW**	**HOS**	**AIC**	**MNW**	**HOS**	**AIC**
Calculating windows	$L_b = 4T_d$ $L_a = 1T_d$ $L_d = (1\text{-}d)T_d$ $d = 0.6T_d$	$[0.5\text{-}2]T_d$ $2tE_1$	~	==	$[0.5\text{-}2]\ T_d$ 2median (tE_1)	~
Guide	BPZ	tP_1	mean(tP_1, tP_2)	Trend	==	==
Searching window	$1.5T_d$	$tE_1 + T_d$	2max(tE_1, tE_2)	$1.5T_d$	max(tE_1)	w1=median(tE_1) w2=median(tE_2) 2max(w1,w2)
Location	After	Around	Around	Around	Around	Around

Table 2 : Thickness and velocities of the layers model used in the simulation

Layer	Thickness (m)		Velocity P-wave	Velocity S-wave
	Left	Right	Vp (m/s)	Vs (m/s)
C1	28.5	14	400	230
C2	16.5	0	1000	580
C3	22.5	22.5	1800	1050
F	10.5		625 - 2500	365 - 1500
S	∞		2500	1500

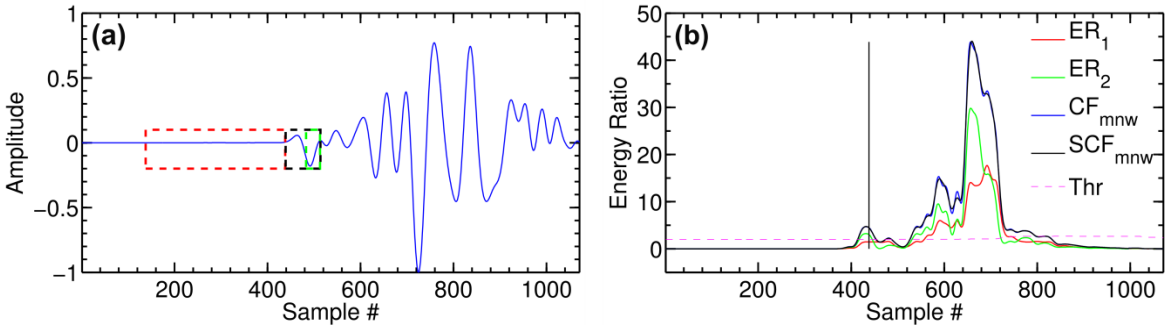

Fig. 1. Illustration of MNW method: (a). normalized free-noisy trace and the three windows (red = before instant t; black = just after instant t; green = after a delay instant t) used on the calculation of CF_{mnw}. (b). Energy ratios (ER1 = energy ratio calculated between the before window and after window; ER2 = calculated energy ratio between delayed window and before window; CF_{mnw} = Characteristic Function of the incorporated energy ratio; CF_{mnw} = Smoothed Characteristic Function; Thr = Threshold). The black line indicates the first break.

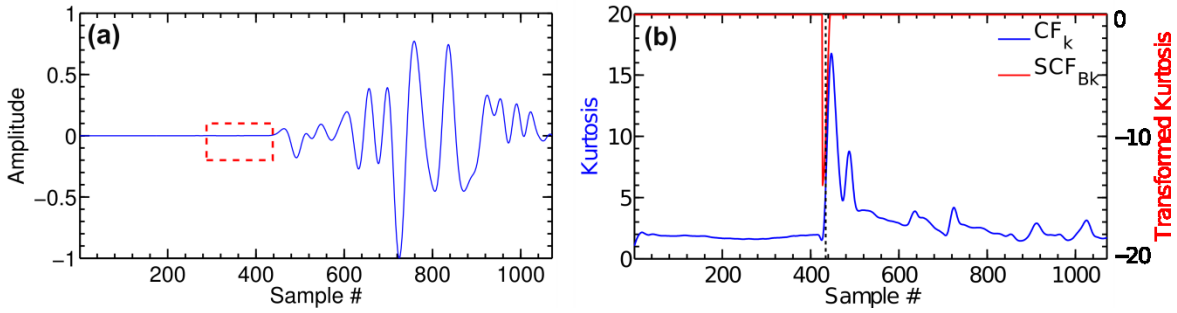

Fig. 2. Illustration of HOS based kurtosis method: (a). normalized free-noisy trace and windows (red rectangle) used for calculating CF_k. (b). the resulting kurtosis CF (blew solid line), and transformed kurtosis based on Baillard procedure (red solid line). The black dashed line indicates the manual pick of first arrival of P-wave.

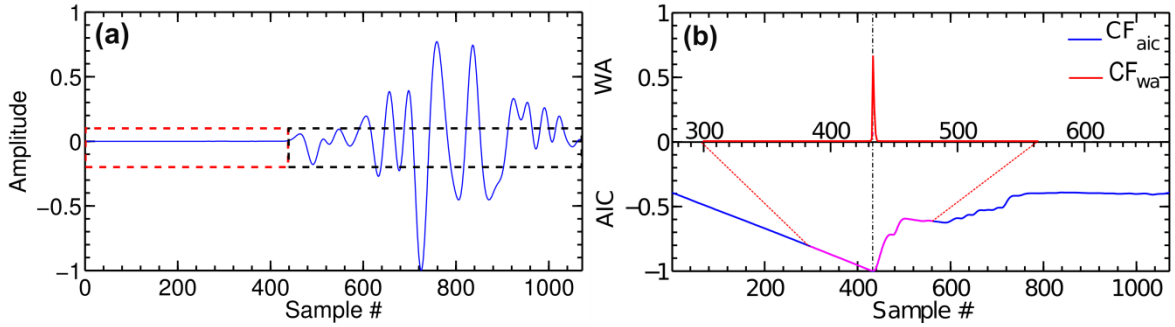

Fig. 3. Illustration of AIC picker based upon Akaike Weights: (a). normalized free-noisy trace and two windows with variable length (red and black dashed rectangles) (b). The CFs based on AIC (blue solid line) and on AW (red solid line). The part of CF_{AIC} used in calculation CF_{wa} is highlighted by purple line. The black vertical dashed line represents the manual pick of the first arrival.

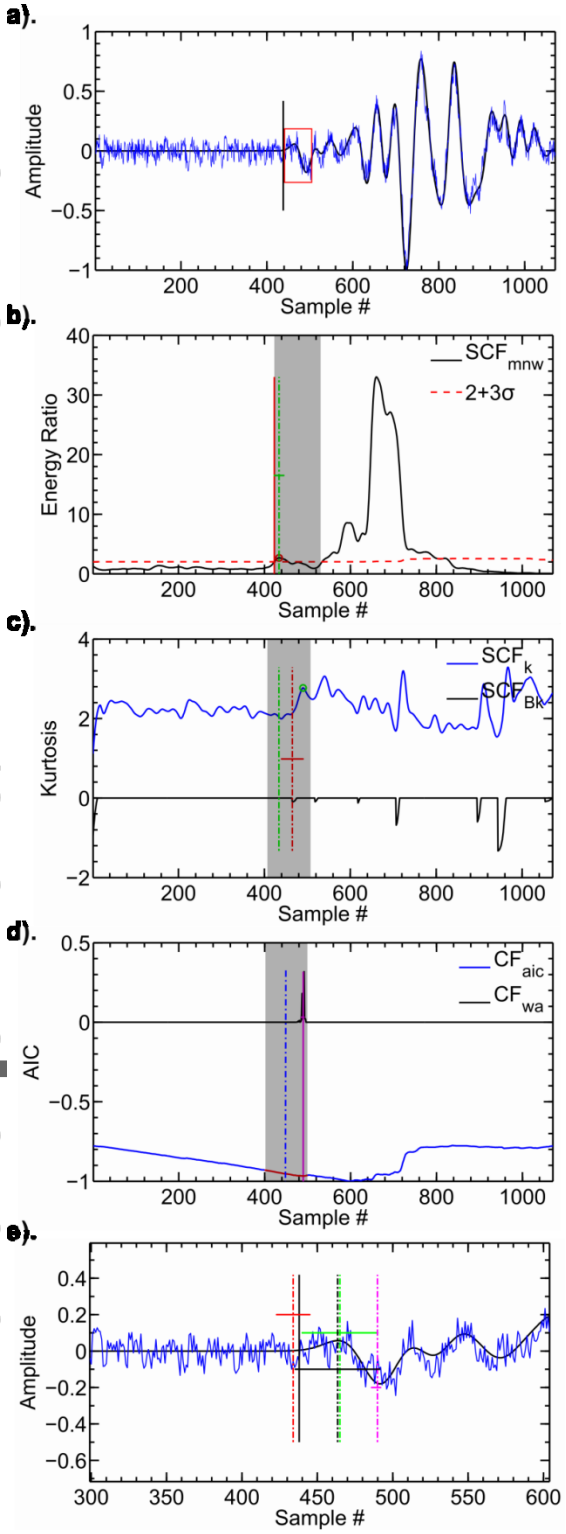

Fig. 4. Illustration of the Single-trace algorithm applied to a synthetic trace: **(a).** Noise-free synthetic trace (black), after adding noise (blue), manual first arrival (vertical black line). The first period of P-wave is framed by the red rectangle **(b).** MNW sub-algorithm topics: threshold (dashed red line), BPZ (vertical red line), picked potential first arrival and the associated error (respectively, vertical pointed and horizontal green line). **(c).** HOS sub-algorithm topics: the guide picker (vertical pointed green line), maximum of kurtosis (small green circle), picked potential first arrival and associated error (respectively, vertical pointed and horizontal red line). **(d).** AIC sub-algorithm topics: the picker guide (vertical pointed blue line), the red part of CF_{aic} is considered for calculating CF_{wa}, the picked potential first arrival and associated error (respectively, vertical and horizontal purple lines). The gray zones in b, c, and d represent the searching windows SW1, SW2, and SW3, respectively. **(e).** Zoom in of the trace in (a) around the first arrival (vertical solid line). The final pick and its error are marked by vertical pointed and horizontal solid lines, respectively. The potential first arrivals and their associated errors picked by the three sub-algorithms are re-delineated on the noisy trace.

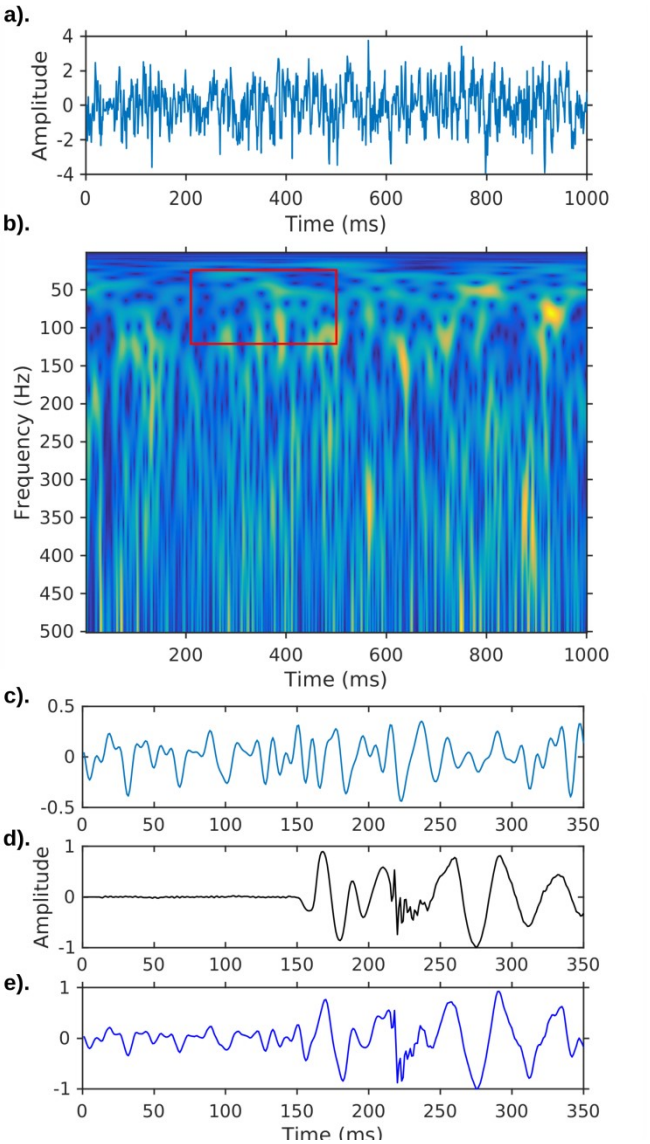

Fig 5. Pseudo-synthetic dataset generating: (a). a random noise trace generated by Gauss-Markov process. (b). S-Transform of the seed trace in (a). (c). inverse S-transform of the selected zone represented by the red rectangle in (b). (d). real trace. (e). noisy trace after adding the noise in (c).

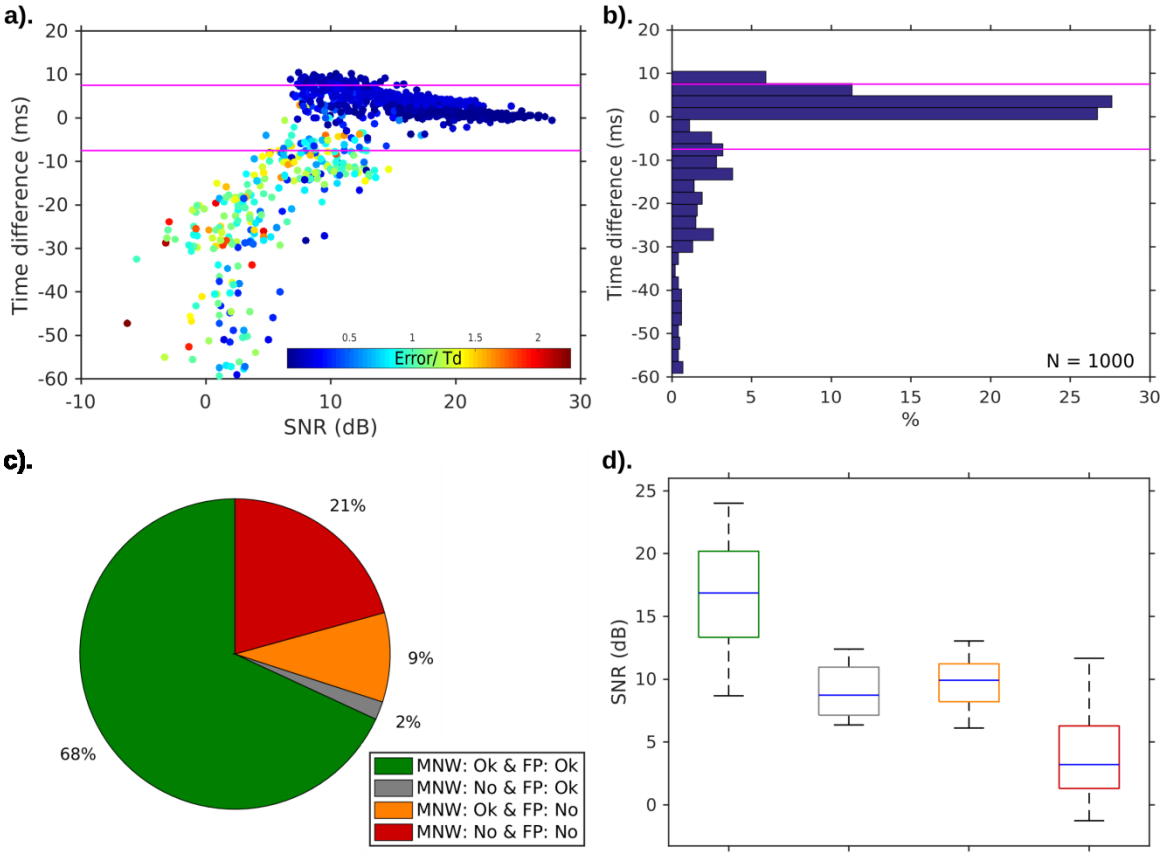

Fig 6. Final picking reliability on pseudo-synthetic dataset: (a). Time differences (automatic - manual) and normalized final error versus SNR plot. (b). histogram of time differences; the purple lines in a and b show the upper and lower levels of acceptable error (±7.5 ms). (c). Time differences pie chart of MNW sub-algorithm and Final Picking (FP); Ok and No signify respectively, the corresponding picker succeeded or not to pick the first arrival in their acceptable error (±Td/4 for FP and ±Td for MNW). (d). Boxplot graphs of the final quality of the picked first arrival classified into groups as in c.

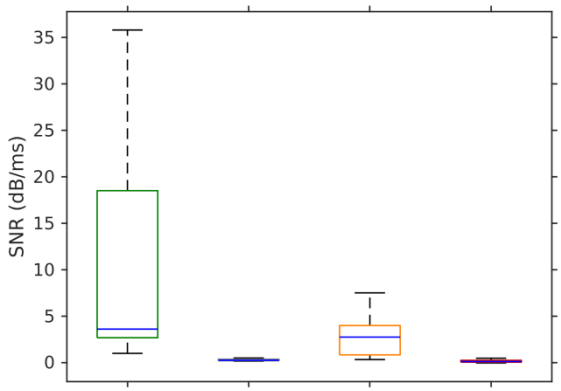

Fig 7. Algorithms consistence evaluation on the groups in Fig 6 via normalization the quality picking by the corresponding error; small values indicate dispersive algorithms (gray group in figure 6) or/and bad quality arrivals (red group in figure 6).

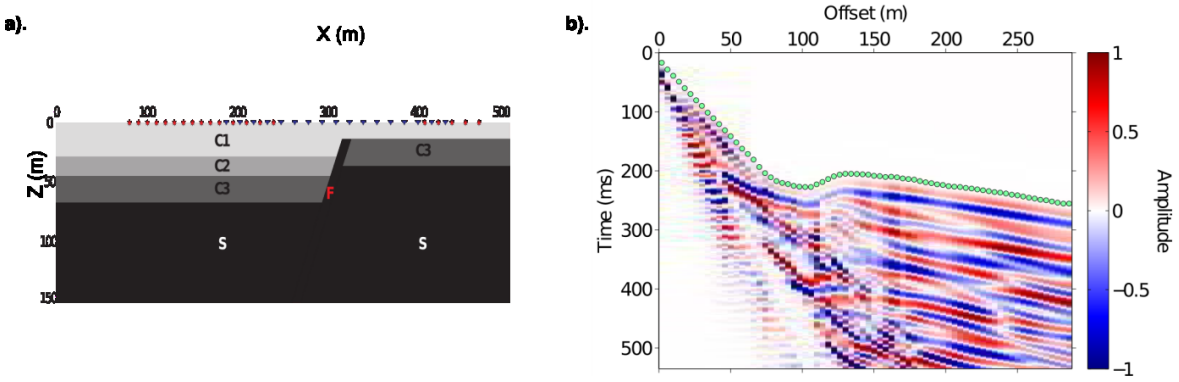

Fig. 8. Numerical simulation: (a). Schematic view of the multi-layer model (layers C1-C3, substratum S, and F page of normal fault) used for generating the synthetic data. The positions of the sources and the receivers are highlighted by red starts and blue triangles, respectively. The thicknesses and velocities are listed in the Table 2. (b). Normalized vertical component of the wavefield simulated by a source located at 198 m from the left side of the model. The small green circles represent the manual picks.

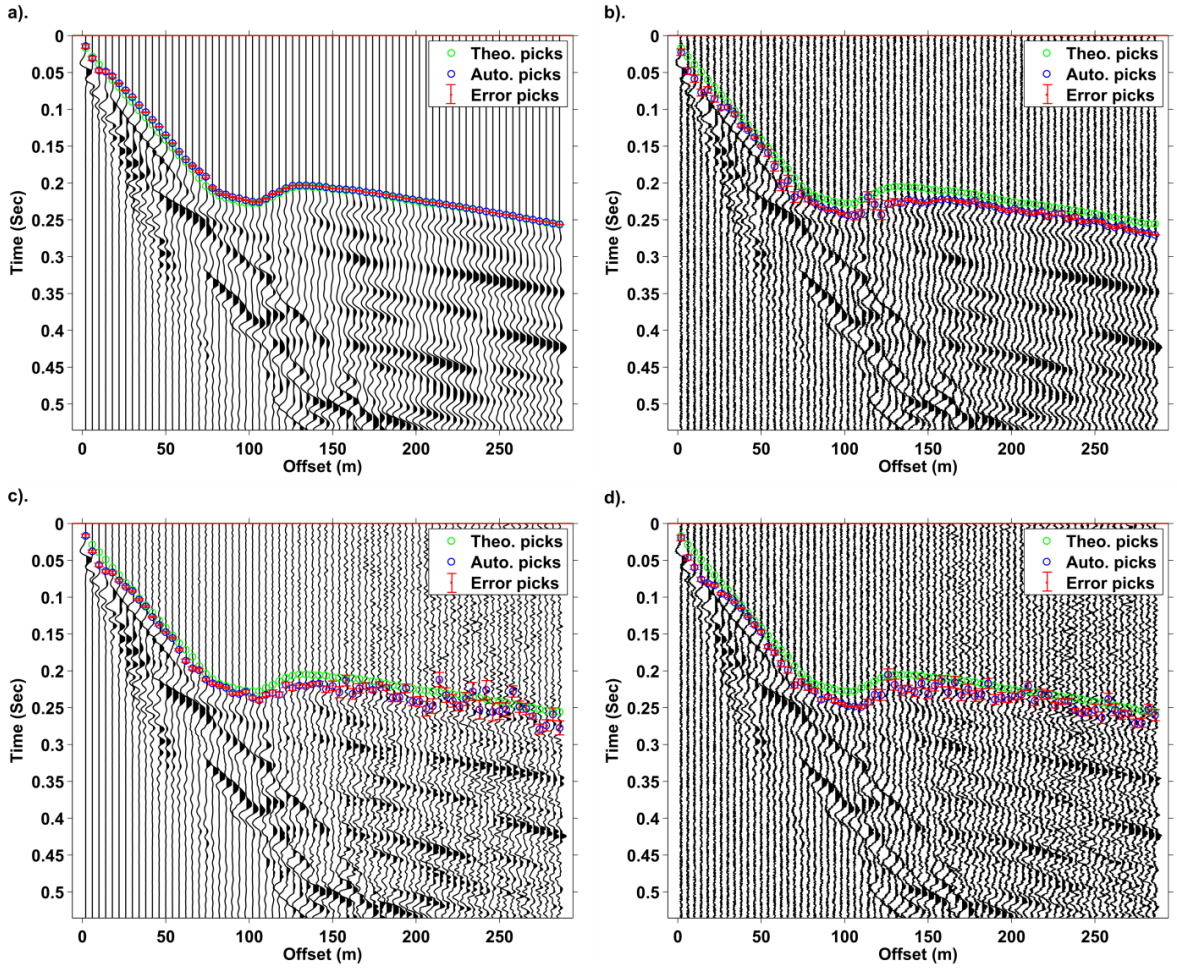

Fig. 8. A synthetic vertical components record with the first arrivals times obtained theoretically (in green) and automatically with their interval errors using the proposed adaptive algorithm (in blue and the error barre in red): (a).Noise-free shot-gather. (b). With 20% random white noise. (c). With random band-limited noise [40-180] Hz. (c). With the noise in (a) and in (b) (random and band-limited noise).

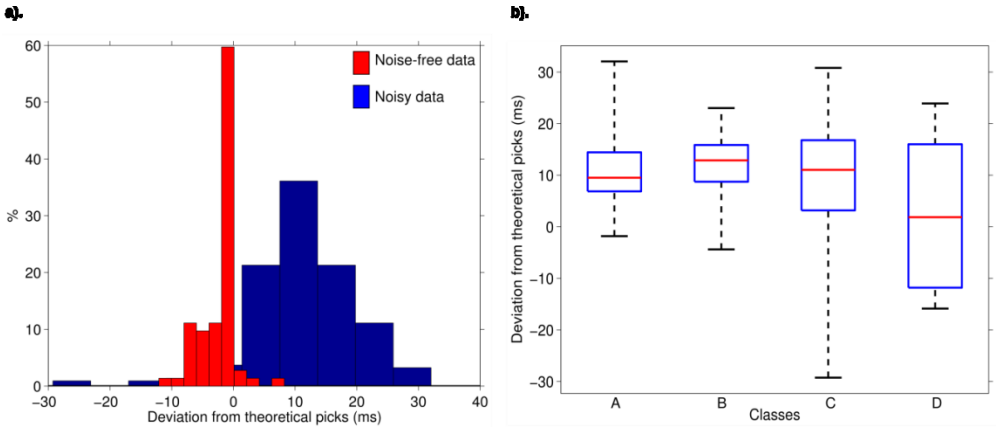

Fig. 9. Statistical analysis: (a). Histograms of differences between automatic and actual picks for noise-free data (in red) and noisy data (blue). (b). Boxplot graphs of the differences for noisy data within the quality classes (A, B, C, and D).

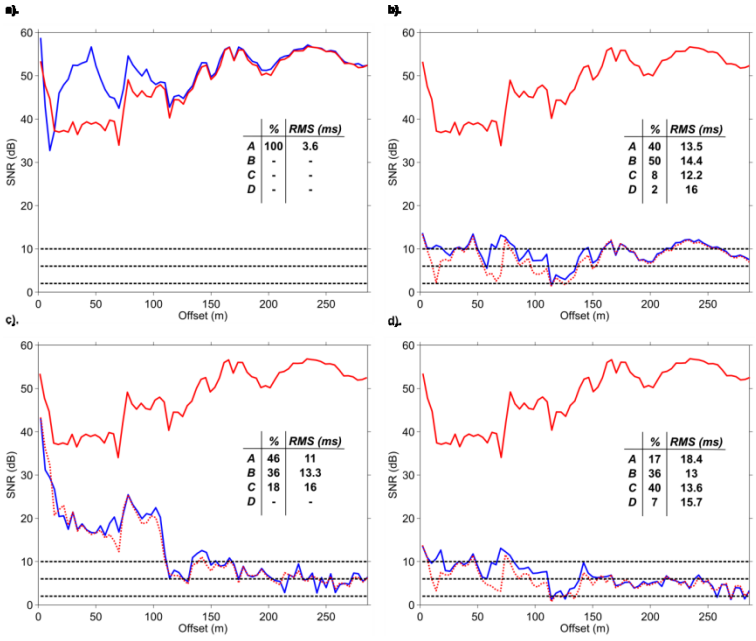

Fig. 10. Quality assessment of automatic and actual picks, respectively in blue and red curves for zero noise (a), 20% random noise added (b), band-limited noise added (c), and random and band-limited noise added (d). The red solid curve represent the quality factor of the actual picks for the noise-free gather, the red pointed curve the same but after adding the noise. The tables in a, b, c, and d show the percent of the traces in each quality class and the related RMS of the differences between the automatic and real picks. The dashed black lines represent the limits of quality categories.

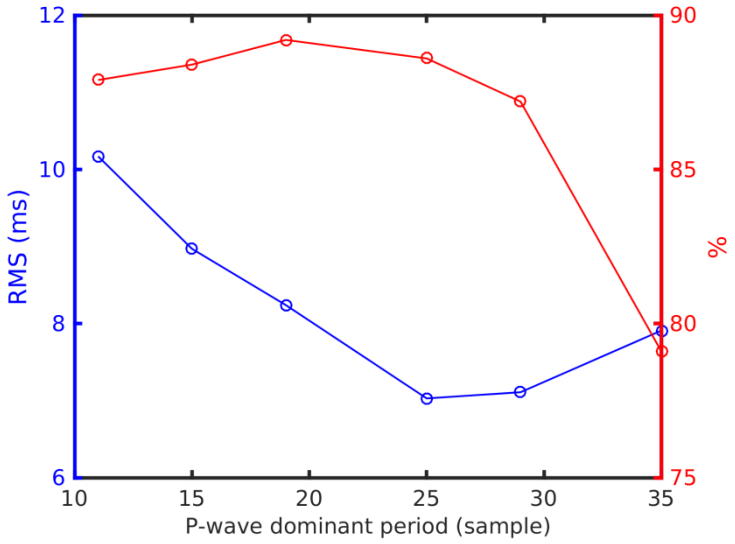

Fig. 11. Trial-and-error results for determining the best first arrival period-length: The curves show values expressed as RMS between automatic and manual picks (left axis) and percentages of hit-rate picking in the manual range-error (right axis).

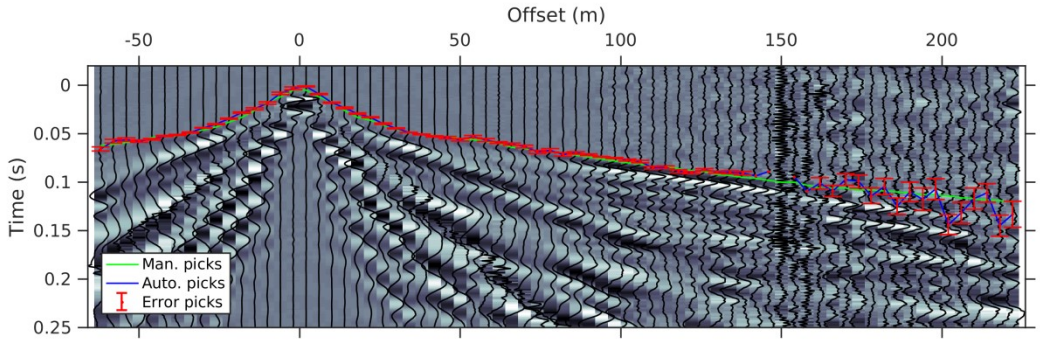

Fig. 12. Shot-gather shown as an example of automatic picking result.

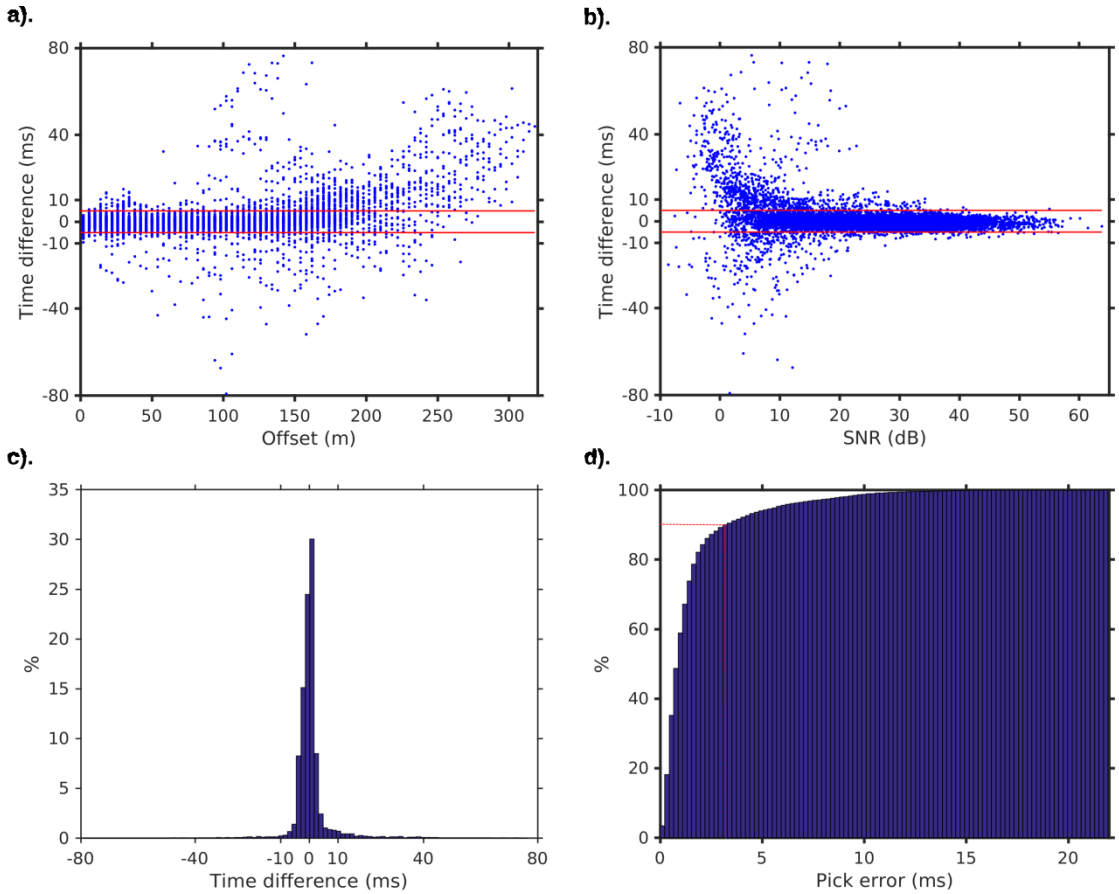

Fig. 13. Basic display and statistics to compare the automatic picking accuracy versus manual picking: (a). Time differences between automatic and manual picks as a function of the offset. (b). Time differences between automatic and manual picks as a function of SNR (quality of first arrivals); the red lines in a and b show the level of the differences at ±5 ms (margin manual picks error). (c). Histogram of the difference between automatic and manual. (d). Normalized cumulative histogram of derived picking errors; the red dashed lines show the level of picked traces at 90% and the corresponding maximum pick error (3 ms).